Lawrence Berkeley National Laboratory
(University of California, University of California)

Year 2008 *Paper LBL*-3058

TEST OF A LIQUID ARGON CHAMBER WITH 20-u m RMS RESOLUTION

S.E. Derenzo A.R. Kirschbaum P.H. Eberhard

R.R. Ross F.T. Sclmitz

Submitted to
Nuclear Instruments and Methods

LBL-3058
Preprint c.1

TEST OF A LIQUID ARGON CHAMBER WITH 20-μm RMS RESOLUTION

S. E. Derenzo, A. R. Kirschbaum, P. H. Eberhard,
R. R. Ross and F. T. Solmitz

July 1974

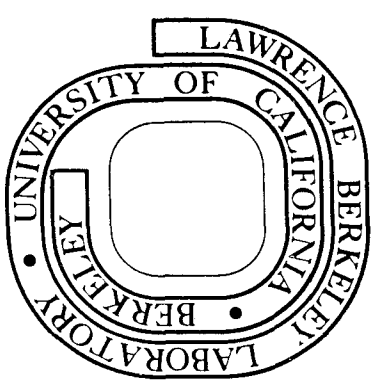

Prepared for the U. S. Atomic Energy Commission
under Contract W-7405-ENG-48

TEST OF A LIQUID ARGON CHAMBER WITH 20-μm RMS RESOLUTION*

S. E. Derenzo, A. R. Kirschbaum, P. H. Eberhard,
R. R. Ross and F. T. Solmitz

Lawrence Berkeley Laboratory
University of California
Berkeley, California 94720

July 1974

ABSTRACT

A measurement of the spatial resolution of a liquid-argon filled chamber was performed with minimum ionizing particles. Two multi-strip chambers with 20-μm strip spacing operating in the ionization mode were used in the experiment. They perform in accordance with a simple model based on electron diffusion. An estimate of the amount of electron diffusion in liquid argon is given and the time jitter distribution has a FWHM of 200 ns. Under best conditions, the spatial resolution is better than 20 μm rms with an efficiency of nearly 100%.

*Work performed under the auspices of the U. S. Atomic Energy Commission.

1. Introduction

In particle physics, many experiments require electronic detectors with high spatial resolution, especially at the highest energies. In response to this need, gas filled chambers have been improved and are now reaching accuracies of the order of 60 to 100 μm rms, using various techniques. These techniques include the measurement of electron drift time[1]), the determination of the geometrical center of gravity of the induced pulse at the cathode[2]), and increases in gas density by high pressures[3]) or low temperatures[4]).

An alternative approach, which leads to even higher spatial resolution, is the use of liquid filled chambers[5]). The advantage of the liquid arises from the ~ 800-fold increase in density over that of the gas, permitting the use of a much smaller thickness, larger ionization statistics, and reduced effect of electron diffusion. Also, the limitation in resolution due to the range of delta rays produced by the incident track is significantly reduced. Unfortunately, the available signal is small because it has so far not been possible to make use of electron multiplication in the proportional or Geiger mode in the liquid for geometries compatible with high resolution[6]). Sparking in a triggered mode has been tried with limited success[7]) and its use still requires the solution of a few problems[8]). In spite of the small signal the ionization mode can be used to explore the potentialities of liquid filled chambers.

We report here on an experiment designed to measure the spatial resolution of liquid-argon filled chambers, and to identify the physical processes that limit their accuracy, such as electron diffusion, amplifier noise, and delta rays. The experiment was performed with minimum ionizing particles using two multi-strip liquid argon filled

chambers, with 20-μm strip spacing (Section 2).

The spatial resolution was determined by measuring the probability of the strips to detect the same particle in each chamber as a function of their relative position (Section 3). Under the best conditions, the spatial resolution for a single strip was measured to be better than 20 μm rms with an efficiency of nearly 100%. The chambers were found to perform in accordance with a simple model based on electron diffusion and amplifier noise (Sections 4,5).

2. Description of the chambers

2.1 LIQUID USED

Liquid argon was chosen in preference to liquid xenon, largely because it is less susceptable to contamination by electronegative impurities. Liquid krypton was not used because of contamination by the radioactive isotope ^{85}Kr.

Special purification of the argon is required since even a 1 ppm contamination of O_2 in liquid argon will reduce the pulse height by a factor of 2 under the conditions of our experiment (a 2.2-mm thick chamber at 2.7 kV/cm)[9]). A schematic diagram of our recirculating purifier is shown in fig. 1. The active elements were the molecular sieve trap (-77°C) and the calcium chips (600°C). Before operation, the chambers were evacuated to a pressure < 10^{-5} mm Hg and were maintained at a temperature of 60°C for about 15 hours. The chambers were then filled with argon gas supplied from the purifier. The gas was liquified inside the chambers by immersing them in a bath of unpurified liquid argon.

2.2 ANODES

The anode pattern, shown in fig. 2, was a series of 24 strips, each 3 mm long and 15 μm wide with a 20-μm center-to-center spacing.

On either side, two larger strips at the same potential as the central strips were used to make the field more nearly uniform in the sensitive region. The pattern was drawn with a digital plotting machine[10]) and reduced 20 fold onto a high-resolution photographic plate to produce a mask. From this mask the final metallic pattern could be contact printed onto metal coated substrates, using standard integrated circuit techniques [11]). The sapphire substrates were coated with approximately 0.1 μm of chromium and 1 μm of gold, the chromium providing bonding between the sapphire and the gold.

Sapphire (crystalline Al_2O_3) rather than glass was chosen as the substrate so that epoxy could be used to attach the anode to the chamber body. Glass was found to crack under such conditions when cooled to -186 °C, the temperature of liquid argon. Ceramic (fused Al_2O_3) was found to provide insufficient bonding to the metallic anode pattern, possibly due to surface irregularities. Wires were also tried[12]) instead of etched strips but this technique was abandoned because of technical difficulties, such as breakage and loss of tension.

2.3 CHAMBER ASSEMBLY

The cathode was a flat glass surface 8 mm in diameter coated with silver, separated from the anode plane by a distance of 2.2 mm. Negative high voltage was supplied to the cathode via a 1 MΩ resistor attached to a kovar wire passing through the glass (fig. 3). The anode strips were each connected to ground through a large resistance. The typical operating voltage was 600 V, corresponding to a field of 2.7 kV/cm. The whole assembly was placed in an enclosure composed of two stainless steel flanges sealed by a copper gasket. Feed-through connectors carried the signals from the anode strips to the outside of the enclosure.

2.4 READOUT

The readout electronics are shown in fig. 4. The strips were connected to low noise charge amplifiers placed within a few inches of the chambers to minimize capacitive load and rf pickup. Total capacitive load was about 30 pF. After being processed by an integrating and differentiating circuit, the signals were sent to a discriminator which produced a standard pulse. The usual time constants of the circuit were 0.2 μs for integration and 2 μs for differentiation. The discriminator level was variable and generally set to select pulses due to a few tenths of a fC (1 fC = 10^{-15} Coulomb) input to the charge sensitive amplifier. The noise level of the electronics was about 0.1 fC rms, equivalent to about 3 μV rms while signals were of the order of 1 fC.

2.5 MONITORING

A strip of ^{241}Am-coated platinum foil was attached to the cathode with conductive epoxy. The pulse height induced by the α particles from that radioactive source provided a monitor of liquid purity independent of beam tracks. The pulse height varied by less than 10% over the time period of a week. We found that within errors, the α pulse height observed on the field flatteners was the same as that observed on the central eight strips connected in parallel. This indicated that the regions of bare substrate between the anodes had little or no effect on the amount of charge collected.

3. Test set-up and procedure

3.1 BEAM

The beam used was a 1.7 GeV/c π^- beam from the Bevatron having an intensity of 10^4 to 10^5 particles/burst. The burst duration was roughly half a second. At the location of the chamber, the beam image was about 2 cm in diameter. Fig. 5 shows the layout of the scintillators

S1, S2, and S3, and the two chambers, denoted X1 and X2. With only S1 and S2 in coincidence, the horizontal beam divergence at the chambers was ±5 mrad rms including the effect of multiple scattering. If in addition S3 was required to be in coincidence, the divergence was reduced to ±3 mrad.

3.2 CHAMBER SET-UP

The chambers were mounted on a stage that held them in an argon bath in a thermally insulated and electrically grounded box. The low noise charge amplifiers were located in this box just above the argon bath. Chambers, stage, argon bath, charge amplifiers, and Scintillator S2 were mounted inside a Faraday cage for additional protection against radio frequency noise.

The chambers were mounted with the plane of the strips normal to the beam and the strips vertical, so as to measure the horizontal position of beam particles. The upstream chamber (X1) was held fixed, while the downstream chamber (X2) could be moved horizontally and vertically across the beam and could be rotated about the beam direction. The relative position of the chambers could be set repeatedly within 10 μm. The two chambers were mounted with anode sides facing each other and placed as close as possible compatible with the free motion of X2. The distance between the centers of their sensitive volumes was 3.7 mm along the beam direction. The material between the two chambers constituted about 0.05 radiation length.

3.3 ALIGNMENT

Initial alignment of the two chambers was achieved by visual observation of fiducial marks scribed on the chamber flanges before assembly. Final alignment was made by maximizing the coincidence rate between single strips in each chamber as a function of the position

and orientation of X2.

3.4 RESOLUTION CURVES

In order to study the spatial resolution of the chambers, the particles were counted only if they triggered the coincidence of S1 S2 and a discriminator connected to one strip of X1, thus defining a very narrow beam of particles. The chamber X2 was moved horizontally across that beam and the ratio r(y) of the rate of coincidences S1 S2 X1 X2 to the rate of S1 S2 X1 coincidences was recorded for each displacement y of the chamber X2. Different curves of this type (called resolution curves) were drawn, corresponding to different values of the relevant parameters, i.e., different numbers of strips of X2 connected together, and the discriminator level on X1 or X2. Sometimes S3 was added to the coincidence to define a beam having smaller angular divergence.

4. Results and Analysis of the Resolution Curves

4.1 GENERAL FEATURES OF THE DATA

Fig. 6 gives examples of two resolution curves measured as a function of the horizontal position. All the resolution curves are of a bell-shape, reasonably well represented by a Gaussian function. Therefore, we summarize the information contained in each r(y) by two parameters only, the height h and the full width at half maximum w and the shape is assumed to be Gaussian.

The best resolution at high efficiency was achieved with the discriminator levels set at 0.5 fC for each chamber. With a beam divergence of 5 mrad we obtained a width w of 80 μm, corresponding to an rms value of 32 μm; we conclude that each chamber had a resolution better than this. The chamber efficiency and the subtraction of the con

tribution of multiple scattering and beam divergence from the resolution are discussed at the end of this section.

When the discriminator level on Chamber X2 was lowered, the height h approached unity, and the width w increased. This is understandable since a lower discriminator level allows a larger fraction of the particles to be counted at all distances and, due to the effects of electron diffusion, far away particles that would not be counted at a higher discriminator level are included. Whenever the beam definition was made narrower, either by requiring a signal from S3 in the coincidence or by raising the discriminator level on X1, the height h increased and the width w decreased as expected.

4.2 THE EFFECTIVE WIDTH

In order to interpret the data in terms of the parameters of the single Chamber X2 we introduce a simple analysis based on a new parameter L, the effective width of a strip in X2, which is just the integral of the measured resolution curve r(y). We show here that L depends on the parameters of X2 but is independent of the distribution of beam particles defined by counters in coincidence with Chamber X1. Let x be the horizontal position of a particle traversing Chamber X2 and p(x) its probability of triggering the discriminator connected to a strip centered at x = 0. Let b(x) be the distribution of such particles defined by the S1 S2 X1 coincidence. b(x) is normalized to 1. When a strip in Chamber X2 is set off-center by a distance x = y, the ratio of S1 S2 X1 X2 coincidences to S1 S2 X1 coincidences is

$$r(y) = \int b(x)\, p(x-y)\, dx. \qquad (1)$$

The effective width of a strip is defined by

$$L = \int r(y)dy = \int p(x)\, dx. \qquad (2)$$

From eq. (2), we see that L does not depend on the beam distribution b(x) and can be measured from the resolution curve r(y) alone. Since r(y) is assumed to be Gaussian, we obtain:

$$L = 1/2\sqrt{\frac{\pi}{\ell n 2}}\ hw = 1.06\ hw. \qquad (3)$$

4.3 COMPARISON OF L WITH A MODEL

Our values of L are plotted on fig. 7, as a function of the discriminator level of X2 expressed in terms of input charge in fC. The data concern single strips in X2, except one point that was taken with two adjacent strips connected together to simulate a wider strip.

The solid curve in fig. 7 represents values of L predicted by a simple model. In this model, the particle deposits a string of ions along its trajectory, the electrons drift along the electric field with a certain amount of diffusion, and land on one or several strips. A discriminator is triggered if and only if the charge deposited on the corresponding strip exceeds a given threshold. There are two constants in the model, a diffusion factor $\tilde{D}$ and the amount of charge q deposited by the particle that escapes recombination and capture by impurities. This diffusion factor $\tilde{D}$ is defined by $\sigma_x = \tilde{D}\sqrt{Z}$ where σ_x is the rms of the electron diffusion distribution orthogonal to the electric field, and Z is the electron drift distance parallel to the electric field[13]). The model fits the data well with $\tilde{D} = 28\,\mu m$ per $mm^{1/2}$ and q = 2.0 fC, as can be seen from fig. 7.

4.4 THE AVERAGE RESOLUTION

The values of L found experimentally could result from different probability functions p(x). In our crude model, p(x) is a square function of unit height for $|x| < L/2$ and zero for $|x| > L/2$. In reality, p(x) is undoubtedly rounded to a certain extent due to amplifier noise, and this

will increase the rms spatial resolutions s_1 and s_2 of Chambers X1 and X2, but will not greatly affect the effective width L. Therefore, although our model may not correctly describe our data in every respect, it does predict the dependence of L on discriminator level rather well (fig. 7).

We further define the average resolution of both chambers as

$$s = \sqrt{\frac{s_1^2 + s_2^2}{2}} \quad . \tag{4}$$

An experimental value of s^2 can be derived from the resolution curve r(y) and a knowledge of the pion beam properties. Let δy be the rms width of a resolution curve r(y). δy^2 is the sum of a term $\delta\hat{b}^2$ due to beam divergence and (including multiple scattering) between the chambers and the two other terms s_1^2 and s_2^2. Hence s^2 is measured by

$$s^2 = \frac{\delta y^2 - \delta\hat{b}^2}{2} \tag{5}$$

The measured resolution δy depends on the joint contribution of both chambers. For the purpose of comparing the measured values of s^2 with the effective width L, we introduce the average effective width $\mathcal{L}$ as

$$\mathcal{L}^2 = \frac{L^2 + L_1^2}{2} \tag{6}$$

where L and L_1 are the effective widths of chambers X2 and X1 respectively. L is determined from eq. (3), while L_1 is obtained from fig. 7, knowing the discriminator level on X1. In the model with p(x) a square distribution of unit height, the relationship between s and $\mathcal{L}$ is given by

$$s^2 = \mathcal{L}^2/12 \quad . \tag{7}$$

4.5 COMPARISON OF s^2 WITH THE MODEL

s_1 and s_2 are expected to depend on the discriminator levels of X1 and X2 respectively. We have obtained s^2 from the resolution curves and eq. (5) for various values of these parameters (fig. 8). Eq. (7) does not fit these data. However, if a constant term of 270 μm^2 is added to the right hand side of eq. (7), the fit to the data is fairly good.

4.6 BEST RESOLUTION AT HIGH EFFICIENCY

We can now use eq. (5) to find the average resolution for the case mentioned in the second paragraph of Section 4. The beam divergence was ±5 mrad, implying that σ_b^2 was 340 μm^2. Both discriminators were at the same level of 0.5 fC, and therefore both chambers are expected to have the same resolution, equal to the average resolution s. s^2 was measured to be (330 ± 60) μm^2, so each chamber had a resolution better than 20 μm. This result is independent of any model for the diffusion, since the only requirement is the hypothesis of equal resolution in the two chambers for equal discriminator levels.

For this situation, we have also measured the overall detection efficiency. Under the assumption that two different strips cannot count unless all strips located in between count also, it is possible to demonstrate[14]) that

$$E = \frac{L - L'}{d} \quad , \tag{8}$$

where E is the overall efficiency for a particle to be counted on any strip of the chamber, L is the effective width defined by Eq. (2), L' is a similar effective width for two adjacent strips in coincidence to detect the same particle, and d is the distance between the centers of two adjacent strips. L was found to be 31 ± 2 μm, L' = 13 ± 2 μm and d was 20 μm. Therefore, the average efficiency E was 0.90 ± 0.15, compatible with 100%.

4.7 RESOLUTION FOR TWO STRIPS IN PARALLEL

Measurements with one strip were dependent on which particular charge amplifier was used, and most measurements reported above are averages over several runs. With two strips, the data were much more reproducible. This was probably related to the fact that the amplifier noise then contributed a smaller fraction of the value of s^2.

For two strips and the discriminator set at 0.33 fC on X2, one strip and the discriminator level at 0.42 fC on X1, and the beam divergence at ±3 mrad, the value of s^2 was found to be (600 ± 100) μm^2. Using figs. 7 and 8, one estimates that s_1^2 was about 350 μm^2, and therefore s_1 was about 30 μm.

5. Additional tests and information

5.1 PULSE HEIGHT SPECTRA

Pulse height data supply additional information about electron diffusion in liquid argon independent of the chamber spatial resolution. In order to check the constants $\tilde{D}$ and q of Section 4, pulse height spectra were recorded for the pulses collected by different numbers of strips of X2 connected together. For this study, the time constants of the readout circuit were changed to 1 μs integration and 5 μs differentiation, and the signals were sent to a pulse height analyzer gated by the coincidence of S1, S2 and X2. Some typical pulse shapes for the time constants used in this experiment are shown in fig. 9.

Pulse height spectra are shown in figs. 10(a) and (b) for one strip and eight adjacent strips respectively. The solid curves superimposed on the data are predictions from the simple diffusion model described in Section 4. In both cases the data are well represented by a diffusion factor $\tilde{D} = 28\ \mu m$ per $mm^{1/2}$ and an initial charge after recombination of q = 2.0 fC (ref. 15). For eight adjacent strips there is a noticeable tail

of events at high pulse heights. Approximately 15% of the events are in this tail, entirely consistent with the ionization distribution expected from the Landau tail. A mean energy loss was used in the simple model and does not account for this tail.

The electron diffusion has been measured in gaseous argon as a function of electric field by Warren and Parker[16]). This data, when extrapolated to the liquid[17]), is in reasonable agreement with our measured value of $\tilde{D}$.

5.2 CHARGE COLLECTION EFFICIENCY

The number of ion pairs produced in liquid argon per unit of energy loss has been measured consistently around 1 ion pair/25 eV under different conditions[18]). Using this value and an energy loss of 2.25 MeV/cm for a minimum ionizing particle, we expect that a charge of about 3.2 fC of each sign is liberated in our 2.2 mm gap. Our analysis shows that the amount of electron charge escaping recombination and capture was about 2.0 fC at an electric field of 2.7 kV/cm. We do not know how much of the difference between these two numbers to ascribe to (a) uncertainties in the liberated charge, (b) errors in our charge measurements, (c) recombination with Ar^+ ions[19]), and (d) capture by residual electronegative impurities[9]).

5.3 MEASURED TIME SPREAD

In order to measure the system time resolution, a time-to-amplitude converter (TAC) was started by a coincidence of Scintillators S1 and S2, and stopped by the first pair of four pairs of strips whose output crossed a discriminator setting of 0.33 fC. The output pulses from the TAC were recorded on a pulse height analyzer. See fig. 11 for the time jitter distribution. Although the time jitter distribution has a FWHM of 200 ns, a 500-ns time gate is necessary to include all the

These measurements are consistent with the simple diffusion model and a drift velocity of 3.3 mm/μs as reported in ref. 20. However, the electronics of the system were not capable of a direct measurement of the drift velocity in this experiment.

6. Conclusions

We have shown that liquid argon filled chambers are capable of detecting minimum ionizing particles with a spatial resolution better than 20 μm rms at an efficiency of nearly 100%. The multi-strip chambers were operated in the ionization mode with expensive low noise amplifiers on each strip, and we consider this the largest single disadvantage to the practical utilization of such chambers.

The performance of the chambers was consistent with a simple model based on the diffusion of electrons and amplifier noise. The transverse electron diffusion factor that best matched the performance was about 30 μm rms per $mm^{1/2}$ of drift. The time jitter distribution had a FWHM of 200 ns, and all the events were included in a 500 ns time interval. The counting rate on each strip was limited by the amplifier recovery time which was of the order of 5 μs.

Based on our experience with two strips in parallel, it is more realistic with present electronics to build chambers with spacings of about 40 μm to increase the signal to noise and hence reliability of operation. Such chambers would have a spatial resolution of about 30 μm rms under the conditions of our test.

Chambers covering several centimeters of linear dimension could be constructed using the same techniques described here. Each centimeter could be covered with 250 strips. The limit to the utilization is to be found in the associated electronics which would at present be bulky and expensive. However, this problem could be overcome by developments in readout electronics.

Acknowledgments

We are indebted to Joe Savignano and Tony Vuletich for building and maintaining our chambers, vacuum system and purifier; to Robbie Smits for assistance in chamber design; to Roger Bangerter, Margaret Garnjost and Horst Oberlack for initial work on the beam; and to Luis Alvarez, Lina Galtieri, Alan Litke, Bernard Sadoulet, and Haim Zaklad for helpful discussions. We thank Dane Anderberg, Bob Hamilton and Will Lawrence for their excellent glass work; Gunner Carlson for his superb welding; Norm Andersen, Uzi Arkadir and Henry Dykman for their skillful production and photo-reduction of the anode mask; and Buck Buckingham, Peter Harding, Ed Lee, John Saarloos, Pete Schwemin, Harold Van Slyke, Garth Smith, Gordon Stutrud, Charles Taylor, and John Taylor for much technical assistance We are especially grateful to Alan Litke, Bernard Sadoulet, Robbie Smits, and John Taylor for assistance in data taking, and we owe a debt of thanks to all the people associated with the operation of the Bevatron whose cooperation made this test possible.

References

1) G. Charpak, D. Rahm, and H. Steiner, Nucl. Instr. and Meth. 80 (1970) 13; G. Charpak, F. Sauli, and W. Duinker, Nucl. Instr. and Meth. 108 (1973) 413; A. Breskin, G. Charpak, B. Gabioud, F. Sauli, N. Trautner, W. Duinker and G. Schultz, Nucl. Instr. and Meth. 119 (1974) 9.

2) R. Grove, K. Lee, V. Perez-Mendez, and J. Sperinde, Nucl. Instr. and Meth. 89 (1970) 257.

3) W. J. Willis, V. Hungerbuehler, W. Tanenbaum, and I. J. Winters, Nucl. and Meth. 91 (1971) 33; S. Dhawan, A. Disco, J. Sandweiss and P. A. Souder, Proceedings of the 1973 International Conference on Instrumentation for High Energy Physics, May 1973, Frascati, Italy, p. 313.

4) M. Atac, Nucl. Instr. and Meth. 95 (1971) 521; M. Atac and W. E. Taylor, Nucl. Instr. and Meth. 118 (1974) 413.

5) L. W. Alvarez, Lawrence Radiation Laboratory Group A Physics Note No. 672 (1968) (unpublished).

6) Proportional electron multiplication in liquid-xenon filled single wire chambers is reliable and has been studied. See S. Derenzo, T. S. Mast, R. A. Muller, and H. Zaklad, Phys. Rev. A9 (1974) 2582. In a series of experiments (described in ref. 12) it was not possible to achieve electron avalanche on an array of 3.5-μm diam electrodes when their spacing was reduced to values smaller than 1 mm. At anode fields below the minimum required for avalanche, there were sparks, probably induced by cold emission at the cathode. One can show, indeed, that the cathode/anode ratio of the fields is proportional to the ratio of wire circumference to wire spacing[12]).

When the 3.5-μm diam electrodes are several mm apart, reliable electron avalanche is possible, but the signal to noise level obtained so far is still not sufficient for development of a high resolution chamber using either drift techniques or the induced pulse at the cathode.

7) A. Riegler, J. Phys. D: Appl. Phys. 2 (1969) 1423.

8) (1) At electric fields of sufficient strength for sparking, cold cathode emission might be a greater source of electrons than the track of the particle to be detected. (2) The spark energy must be carefully limited to protect the narrow electrodes. (3) A clearing field is needed to limit recombination, and efforts must be made so that this field does not sweep the electrons from the gap before the high voltage is applied.

9) D. W. Swan, Proc. Phys. Soc. 83 (1964) 659. Swan found that in liquid argon the number of free electrons N(X) surviving after drifting a distance X(cm) was given by $N(X) = N(0)\ e^{-8Xc/E}$, where c is the O_2 contamination in ppm and E is the electric field in kV/cm.

10) The plotting machine used was located at the Lawrence Livermore Laboratory, Livermore, CA 94550. It has a 2.54 μm step size, a 1.5 m × 2.5 m plotting surface and was manufactured by the Gerber Scientific Instrument Co., Hartford, Conn.

11) Lockheed Integrated Circuits Division, P.O. Box 504, Sunnyvale, CA 94808.

12) S. E. Derenzo, A. Schwemin, R. G. Smits, H. Zaklad, and L. W. Alvarez, Lawrence Berkeley Laboratory Report No. LBL-1791 (April 1973), Proceedings of the 1973 International Conference on Instrumentation for High Energy Physics, May 1973, Frascati, Italy, p. 305.

13) The usual diffusion constant D is defined by $\sigma_x = \sqrt{2DT}$ where T is the drift time. Thus our value $\tilde{D}$ = 30 μm per $mm^{-1/2}$ corresponds to D = 1500 $mm^2\ s^{-1}$. The drift velocity is 3.3×10^5 cm s^{-1} at 2.7 kV/cm (ref. 20).

14) S. Derenzo and P. Eberhard, Efficiency analysis for liquid-filled high-resolution multi-strip ionization-mode chambers, Lawrence Berkeley Laboratory, Group A Physics Note. No. 785 (1974) (unpublished).

15) These data have been corrected for the retention of electron charge by the Ar^+ ions. See ref. 17 for a description and calculation of this effect. When the anode spacing d is very small compared to the anode-cathode spacing Δ, the fraction of electron charge f retained by the Ar^+ ions is very small. On the other hand, when $d \gg \Delta$, then f = 0.5. For a single strip (d/Δ = 0.0091), f = 0.115. For eight strips in parallel (d/Δ = 0.109), f = 0.115. (Note that in ref. 12, f was erroneously assumed equal to 0.5 in all cases.)

16) R. W. Warren and J. H. Parker, Phys. Rev. 128 (1962) 2661.

17) S. Derenzo, Electron diffusion and positive ion charge retention in liquid-filled high-resolution multi-strip ionization-mode chambers, Lawrence Berkeley Laboratory, Group A Physics Note No. 786 (1974) (unpublished).

18) The following measurements have been made in liquid argon: (1) 1 pair/26.0 eV for 5-MeV α particles (heavily ionizing) [D. W. Swan, Proc. Phys. Soc. 85 (1965) 1297]. (2) 1 pair/25.7 ± 3 eV for x-rays [H. A. Ullmaier, Phys. Med. Biol. 11 (1966) 95]. (3) 1 pair/22.5 ± 3 eV for 1.5 MeV x-rays [N. V. Klassen and W. F. Schmidt, Can. J. Chem. 47 (1969) 4286]. (4) 1 pair/$23.6\ ^{+.5}_{-.3}$ eV for 1-MeV electrons [M. Miyajima, T. Takahashi, S. Konno, T. Hamada, S. Kubota, H. Shibamura, and T. Doke, Phys. Rev. A9 (1974) 1438].

19) The measurements for recombination of ion pairs in liquid argon by J. H. Marshall, Rev. Sci. Instr. 25 (1954) 232, for 0.6-MeV electrons, and by M. Miyajima et al., see ref. 18(4) for 1.0-MeV electrons, lead to contradictory estimates for the recombination loss at 2.7 kV/cm. (29% and 12% respectively.)

20) L. S. Miller, S. Howe, and W. E. Spear, Phys. Rev. 166 (1968) 871.

FIGURE CAPTIONS

Fig. 1. Schematic diagram of recirculating purifier.

Fig. 2. Gold anode pattern (light) on sapphire substrate (dark).

(a) Overview showing fanout to circular ring of bonding pads (18 mm diam.).

(b) Enlargement of central region showing 24 strips between two broad electrodes used to make the field more uniform.

(c) Further enlargement showing 15 μm wide strips on 20 μm centers.

Fig. 3. Schematic of chamber construction.

(a) Cutaway of chamber showing feedthroughs, fill pipe, demountable seal using copper gasket, and cathode.

(b) Enlargement of anode region, showing stainless steel beam window, sapphire disk, copper guard electrode, cathode, and α source.

Fig. 4. Readout electronics used in experiment.

Fig. 5. Plan view showing beam, scintillator and chamber layout. Liquid argon chambers are labeled X1 and X2. Horizontal dimensions of scintillators S1, S2, S3 transverse to the beam were 25 mm, 1.6 mm, and 6.4 mm, respectively.

Fig. 6. Measured values of r for single strips in X1 and X2 vs the horizontal position of chamber X2 relative to X1. r is the ratio of S1 S2 S3 X1 X2 coincidences to S1 S2 S3 X1 coincidences. X1 threshold ≈0.4 fC.

Fig. 7. Effective width L vs discriminator setting. Curves are predictions based on the simple model and parameters discussed in section 4.3. Dashed curve, two strips in parallel. Solid curve, single strip.

Fig. 8. Square of the average resolution s^2 vs the square of the effective width $\mathcal{L}^2$. Solid line is $s^2 = \mathcal{L}^2/12$. Dashed line is $s^2 = \mathcal{L}^2/12 + 270\ \mu m^2$.

Fig. 9. Pulses obtained from 8 adjacent strips in chamber X2 attached to one amplifier. Oscilloscope was triggered by a coincidence between scintillators S1 S2 S3 and one strip in chamber X1. Integration/differentiation time constants were:

(a) 0.2 μs/2 μs and (b) 1 μs/5 μs.

Fig. 10. Amplitude distribution of pulses in chamber X2 in coincidence with scintillators S1 S2 S3 and chamber X1.

(a) One strip in X1 and one strip in X2.

(b) Eight strips in X1 and eight strips in X2. Curves are predictions based on the simple model and parameters discussed in section 4.3.

Fig. 11. Time lapse distribution between coincidence of scintillators S1 S2 and the first pair of strips from X2, as explained in section 5.3.

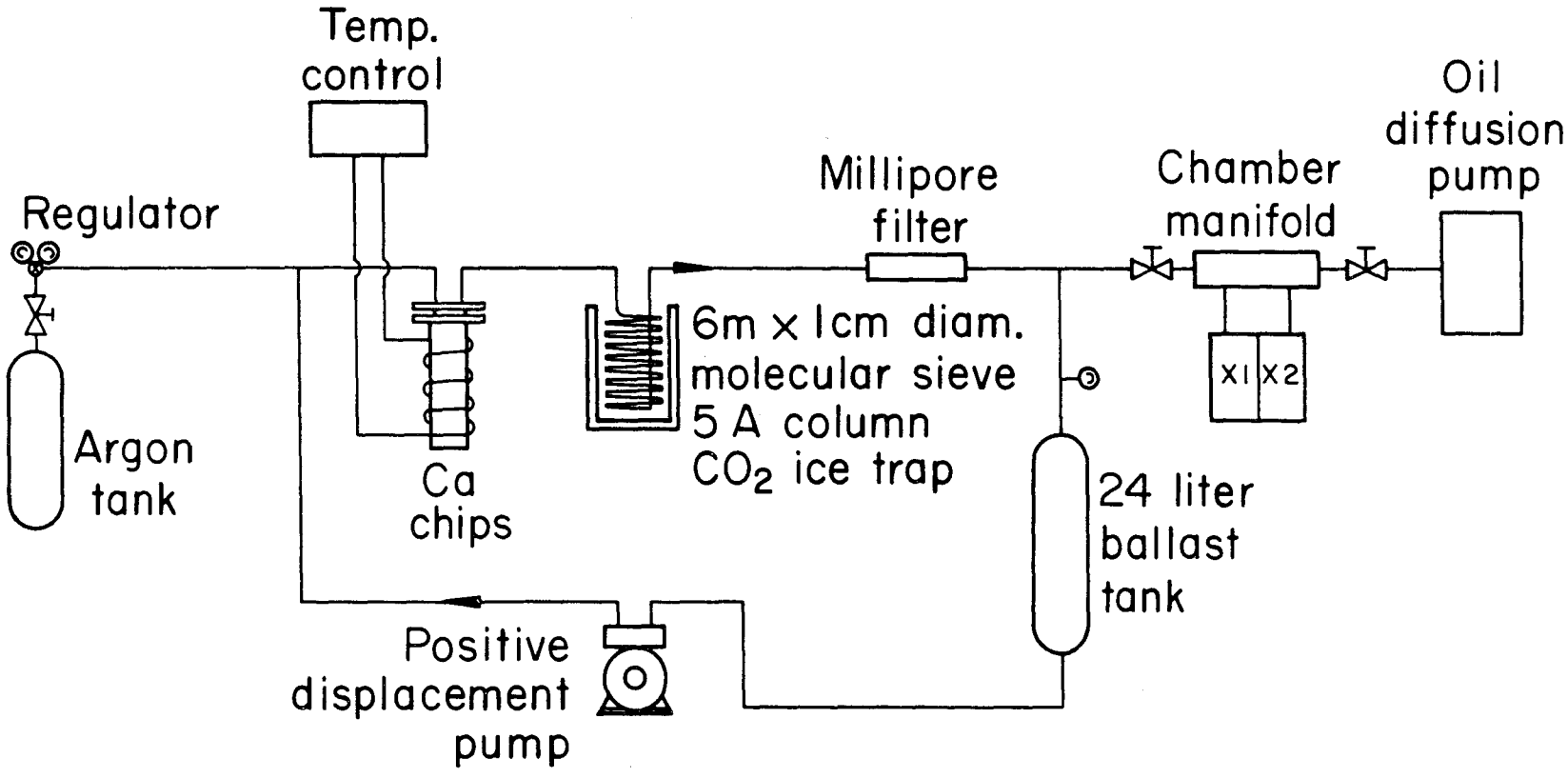

Fig. 1

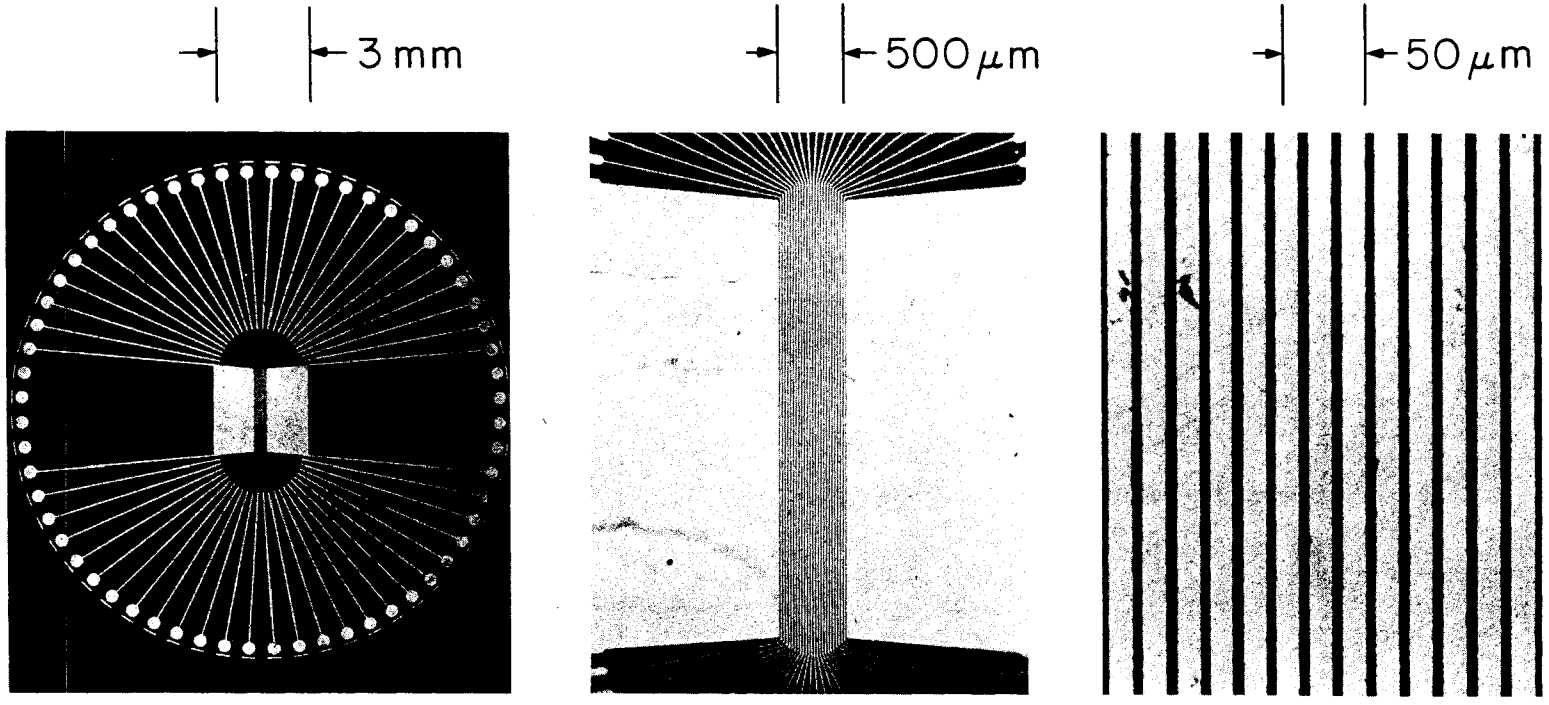

XBB 748-5884

Fig. 2.

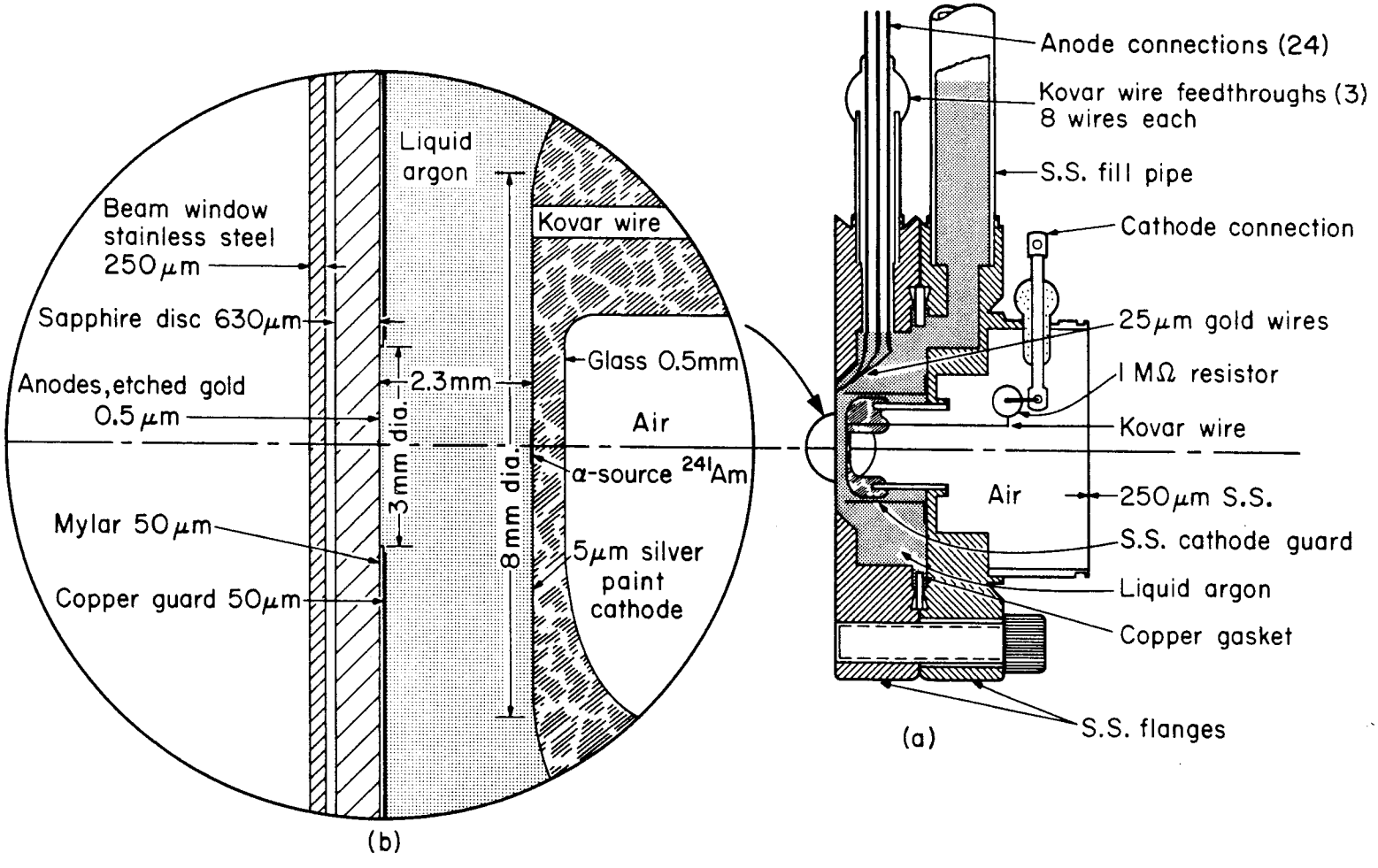

XBL 748-3779

Fig. 3

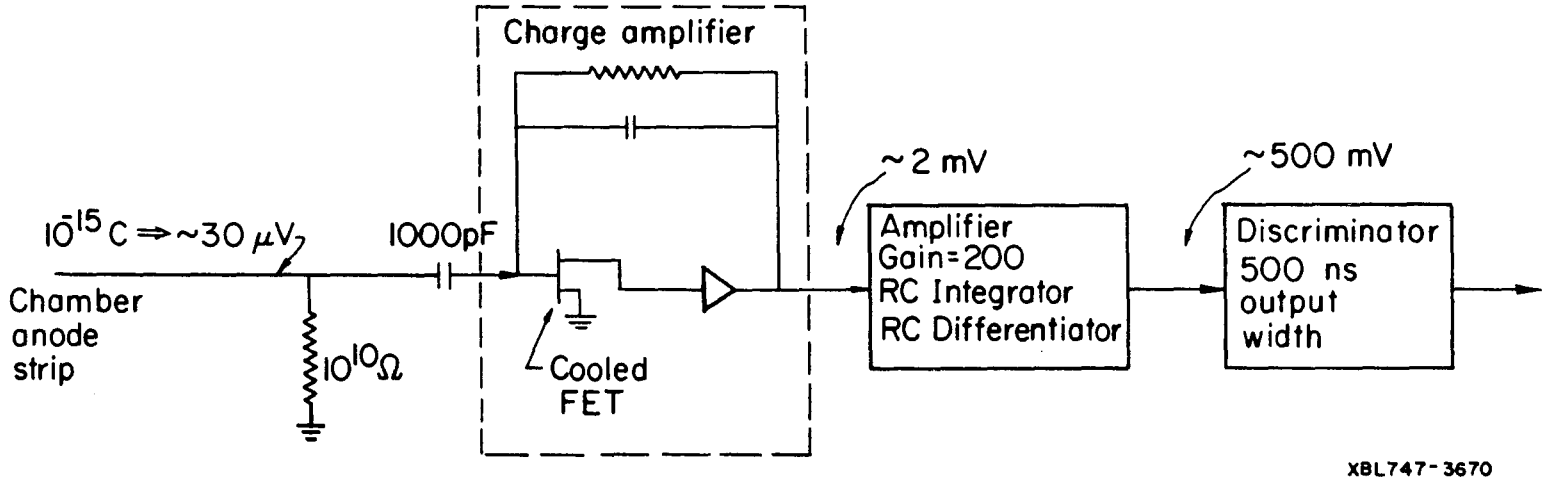
Charge amplifier
10^{-15} C ⇒ ~30 μV
1000pF
Chamber
anode
strip
$10^{10}\Omega$
Cooled
FET
~2 mV
Amplifier
Gain=200
RC Integrator
RC Differentiator
~500 mV
Discriminator
500 ns
output
width
XBL747-3670

Fig. 4

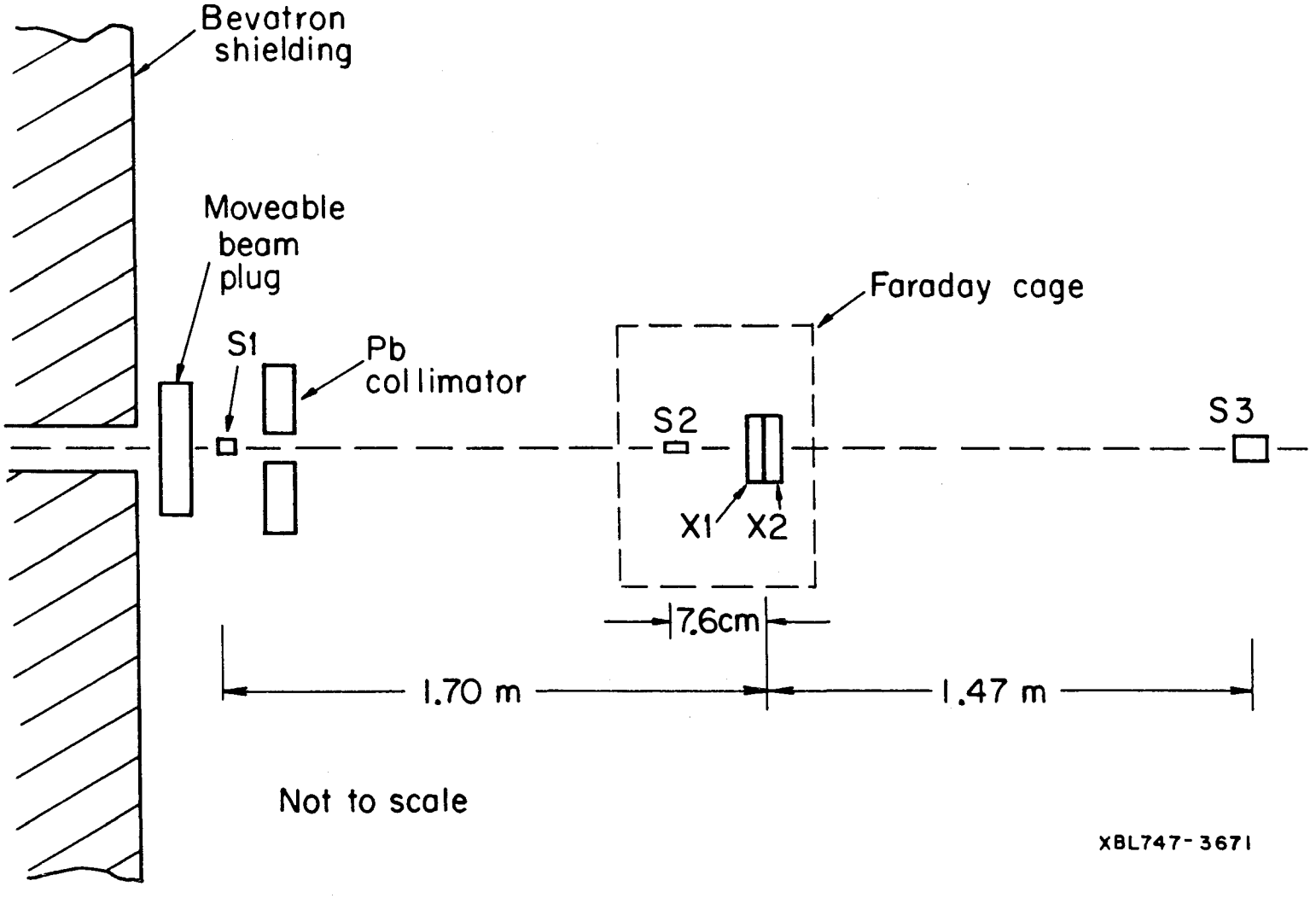

Fig. 5

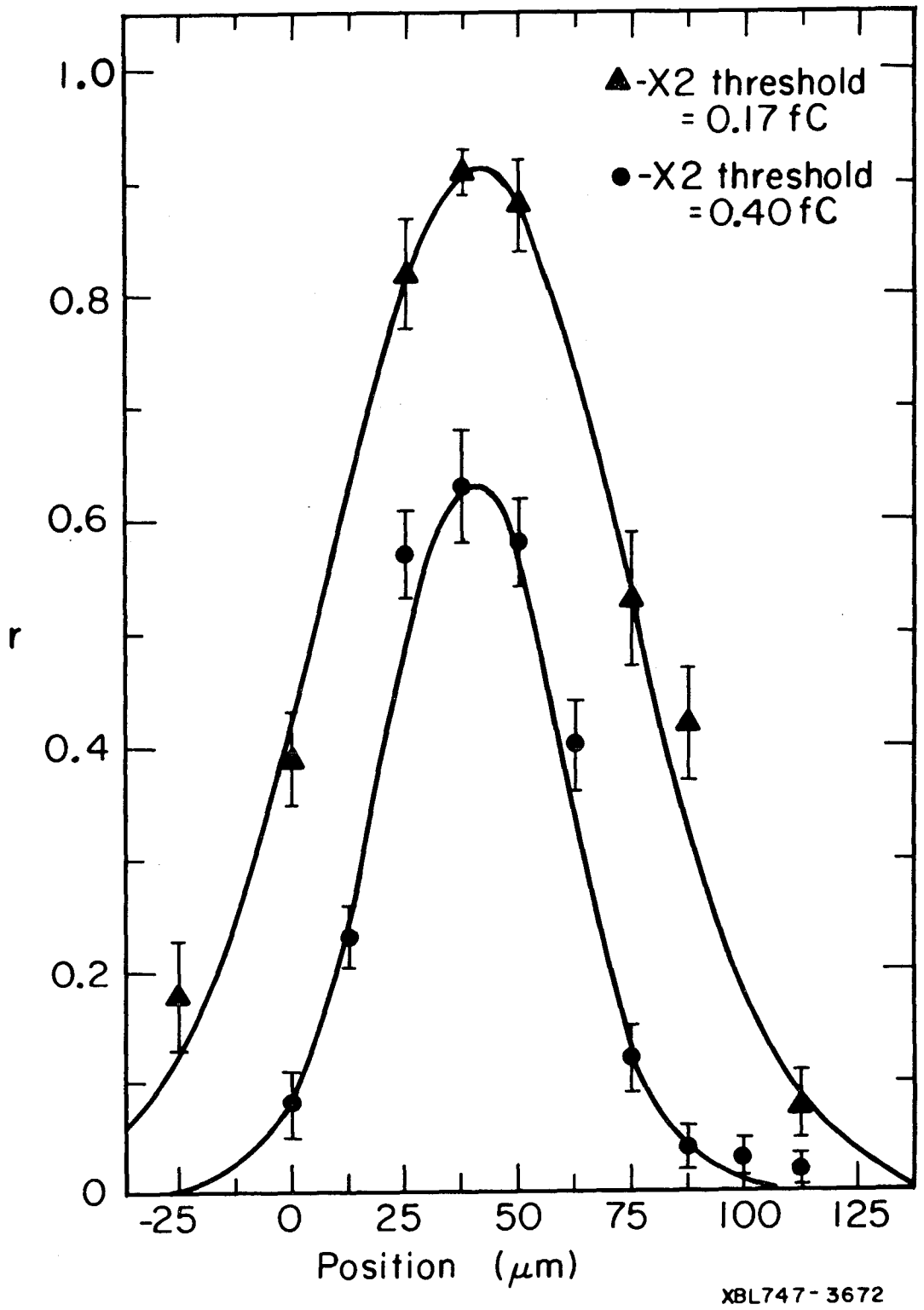
1.0
0.8
0.6
0.4
0.2
0
r
▲-X2 threshold
= 0.17 fC
●-X2 threshold
= 0.40 fC
-25
0
25
50
75
100
125
Position (μm)
XBL747-3672

Fig. 6

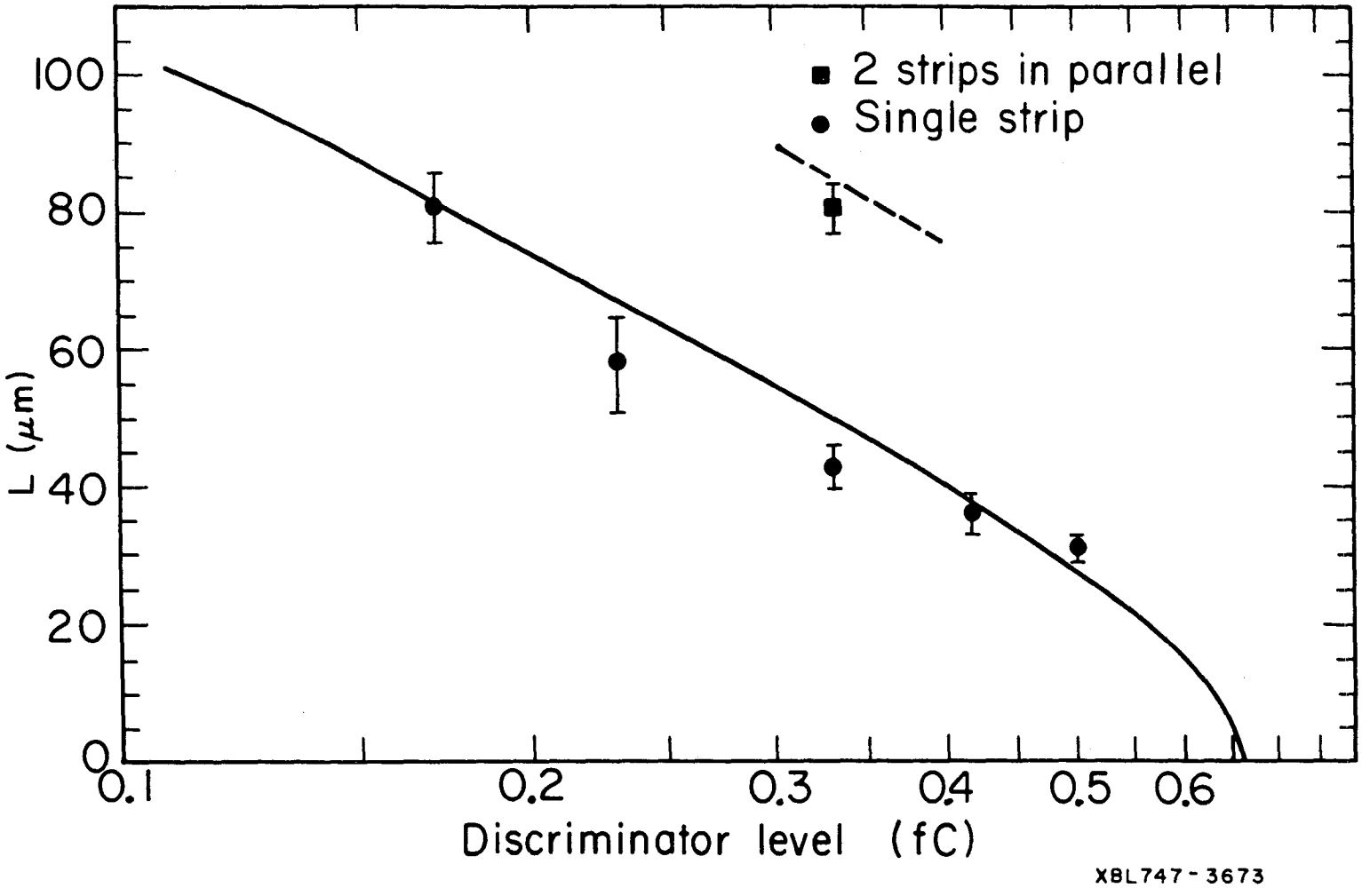
2 strips in parallel
Single strip
100
80
60
40
20
0
L (μm)
0.1
0.2
0.3
0.4
0.5
0.6
Discriminator level (fC)
XBL747-3673

Fig. 7

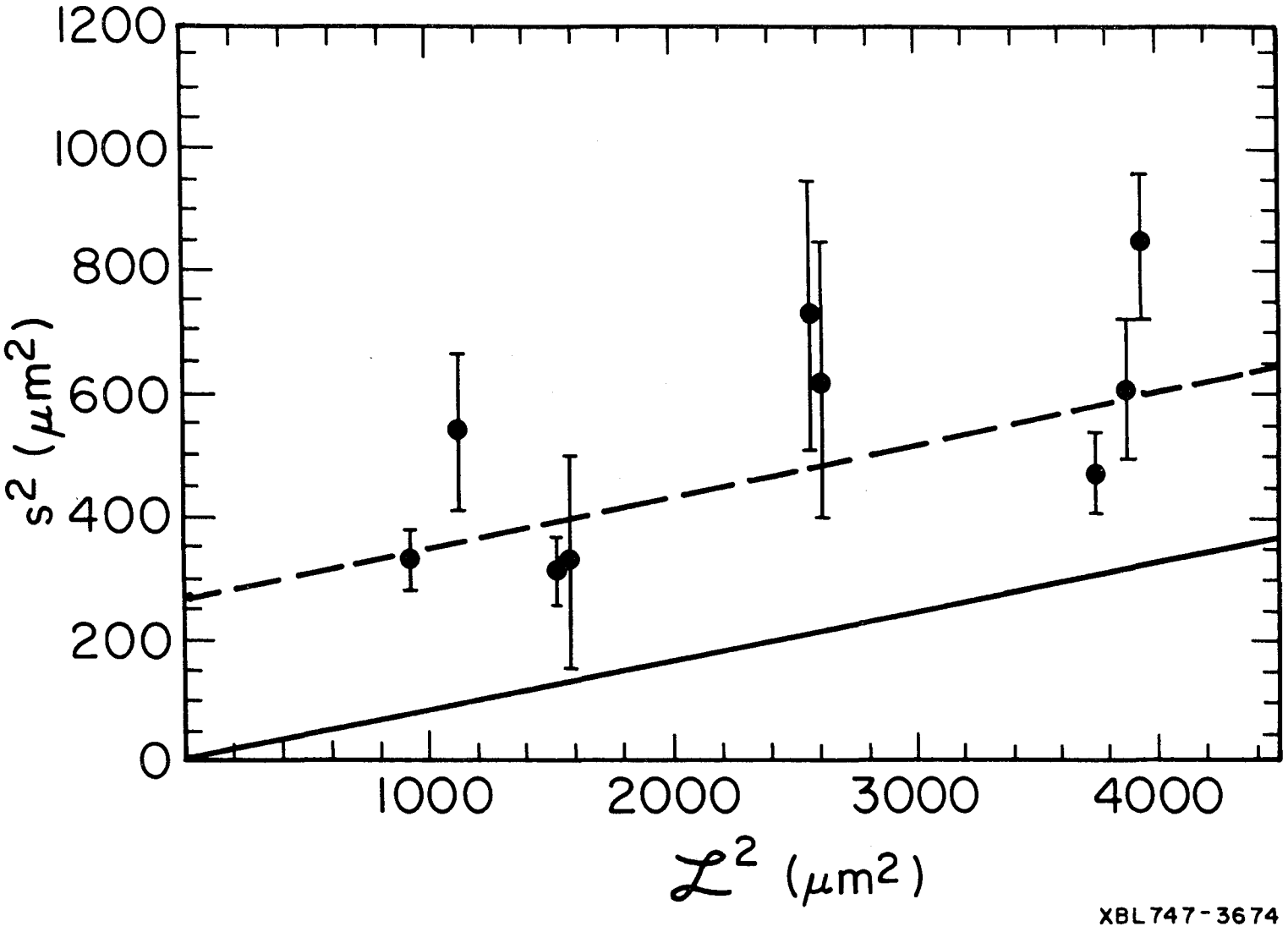
1200
1000
800
600
400
200
0
s^2 (μm^2)
1000
2000
3000
4000
$\mathcal{L}^2$ (μm^2)
XBL747-3674

Fig. 8

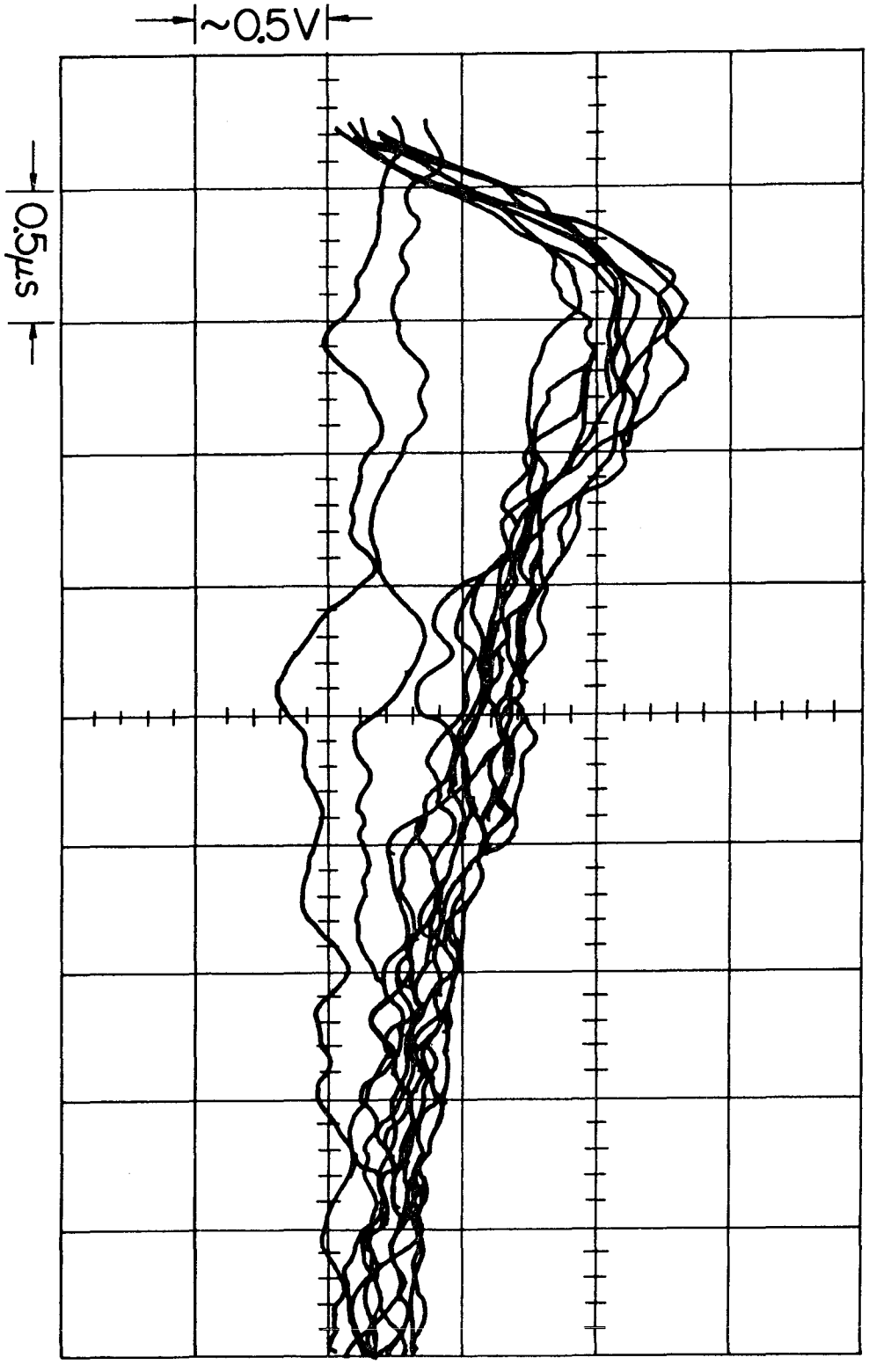

Fig. 9a

XBL747-3675

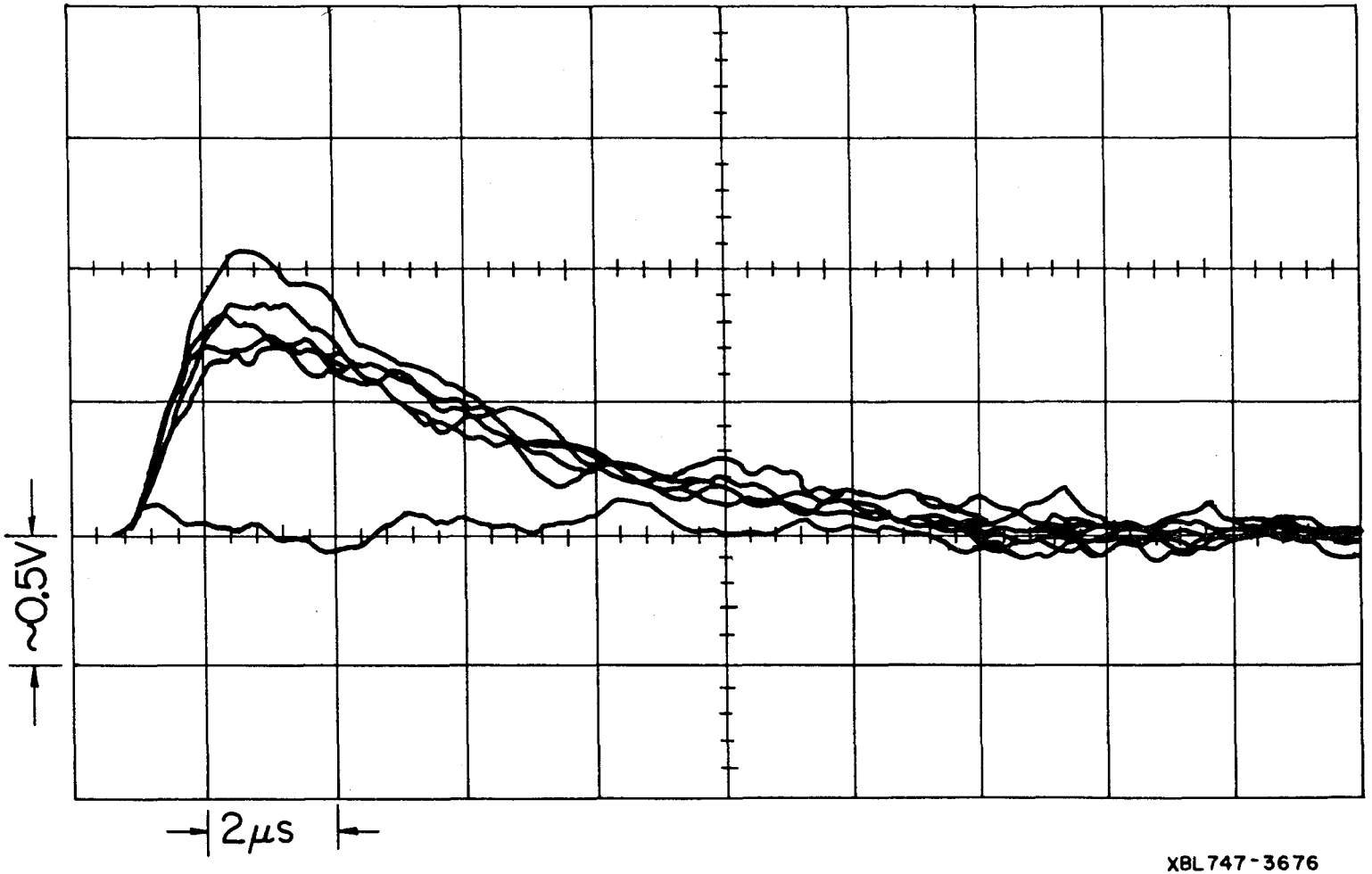

Fig. 9b

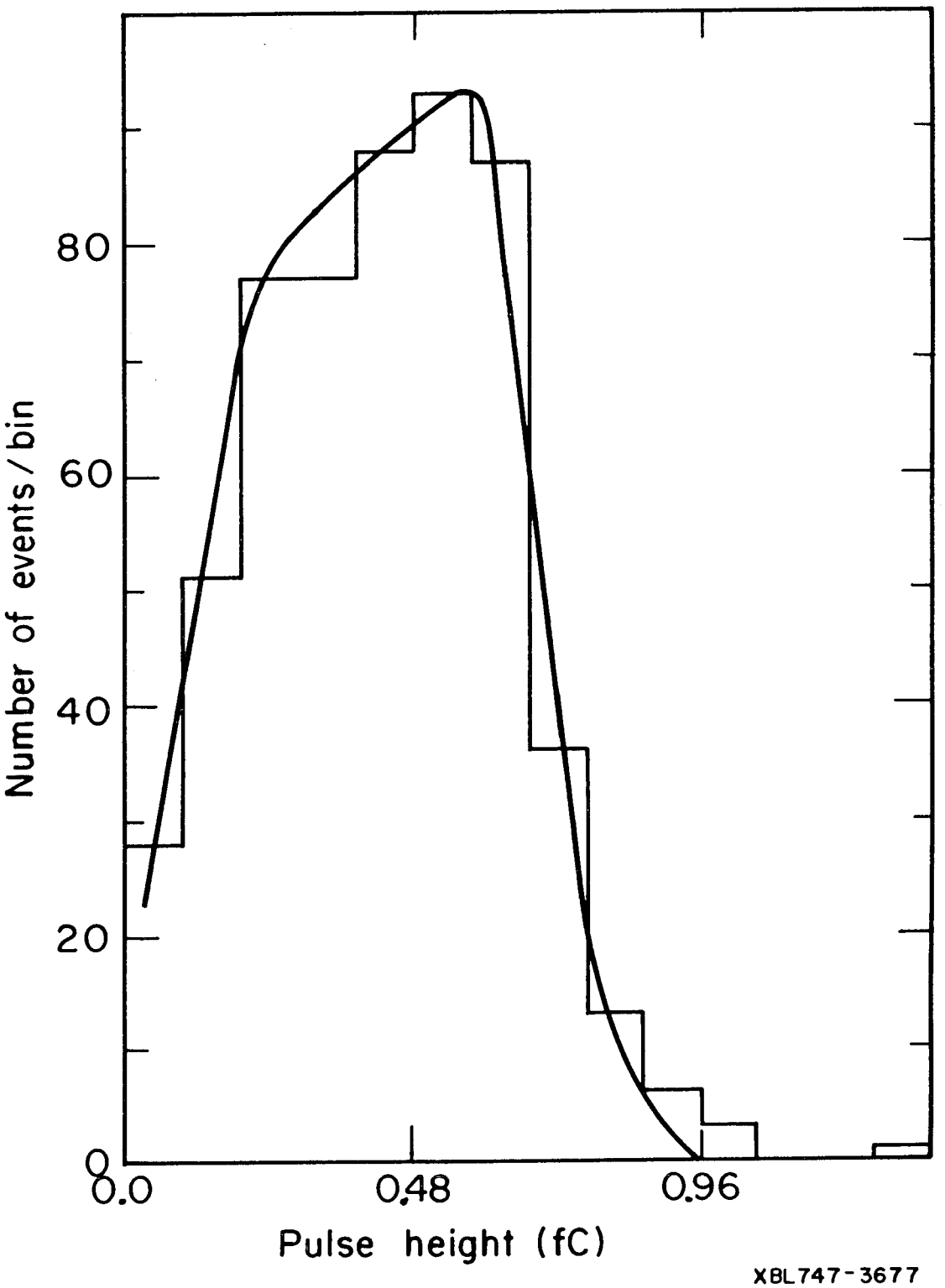

Fig. 10a

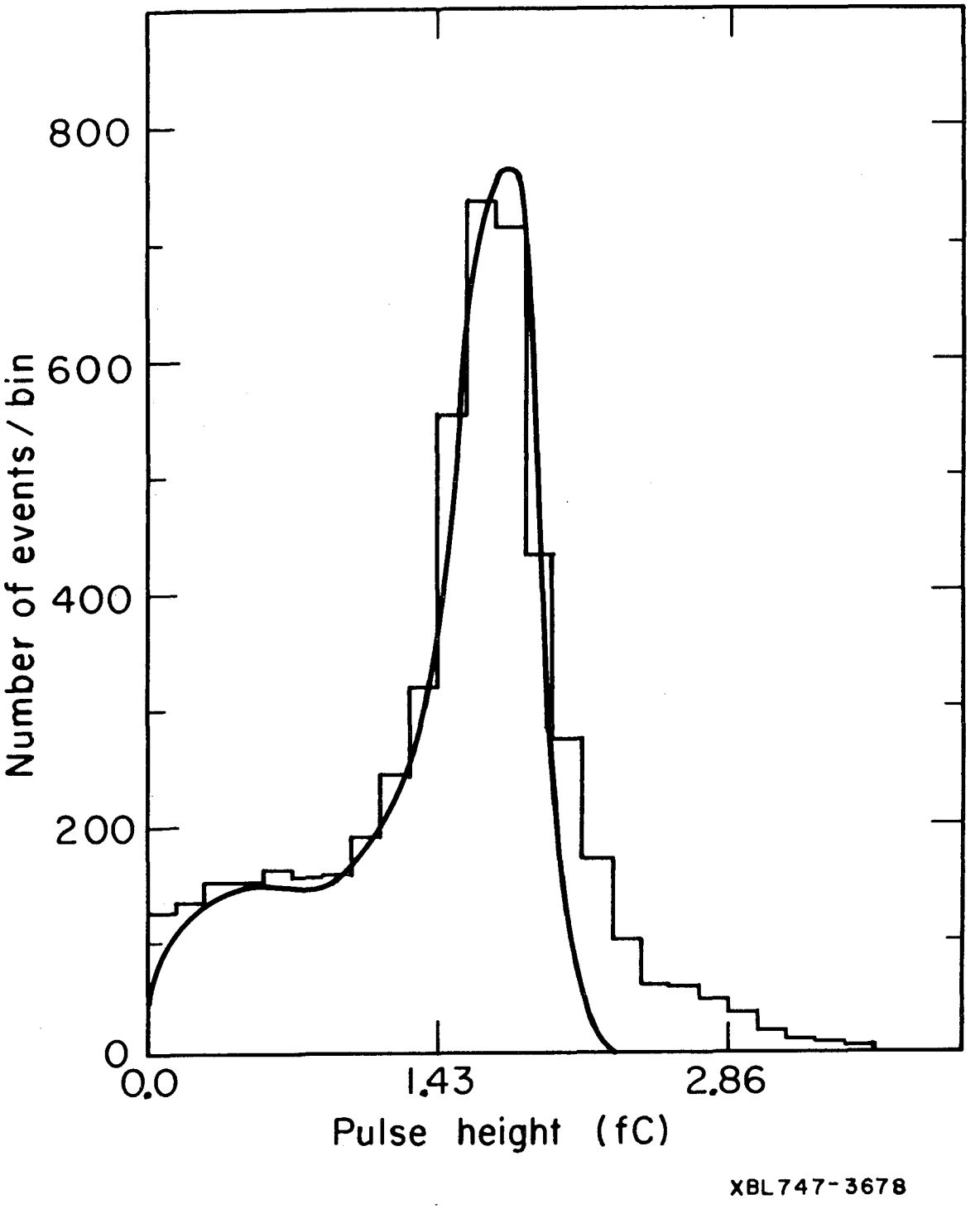
800
600
400
200
0
Number of events / bin
0.0
1.43
2.86
Pulse height (fC)
XBL747-3678

Fig. 10b

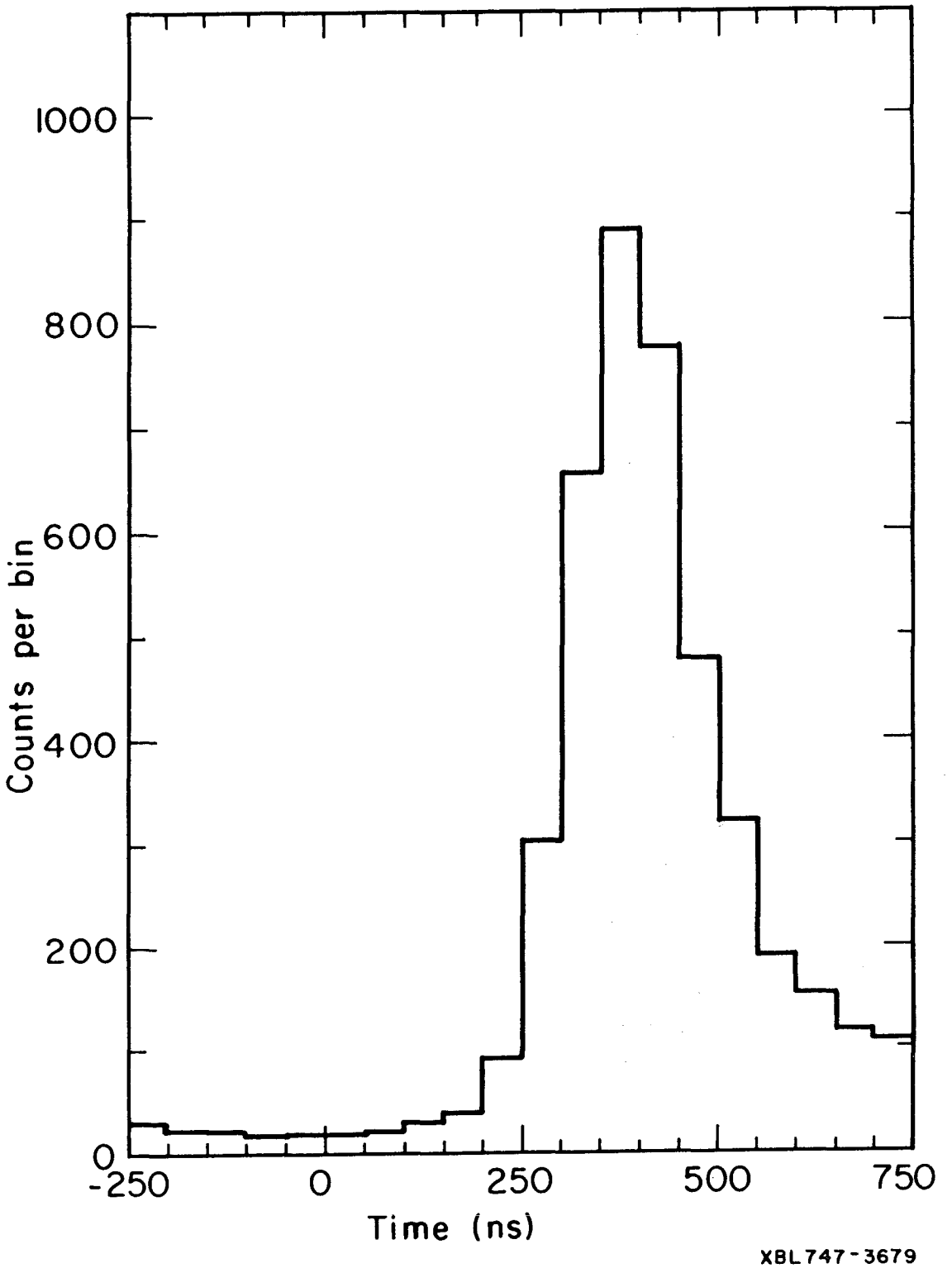
1000
800
600
400
200
0
Counts per bin
-250
0
250
500
750
Time (ns)
XBL747-3679

Fig. 11